TU Delft

Delft University of Technology

Analysis of polydihydrosilane crystallization by excimer laser annealing

Trifunovic, Miki; Sberna, Paolo; Shimoda, T; Ishihara, Ryoichi

Publication date
2017

Document Version
Final published version

Published in
Thin Solid Films

Citation (APA)
Trifunovic, M., Sberna, P., Shimoda, T., & Ishihara, R. (2017). Analysis of polydihydrosilane crystallization by excimer laser annealing. *Thin Solid Films*, *638*, 73-80. https://www.sciencedirect.com/science/article/pii/S0040609017305321

Important note
To cite this publication, please use the final published version (if applicable).
Please check the document version above.

Copyright
Other than for strictly personal use, it is not permitted to download, forward or distribute the text or part of it, without the consent of the author(s) and/or copyright holder(s), unless the work is under an open content license such as Creative Commons.

Takedown policy
Please contact us and provide details if you believe this document breaches copyrights.
We will remove access to the work immediately and investigate your claim.

This work is downloaded from Delft University of Technology.
For technical reasons the number of authors shown on this cover page is limited to a maximum of 10.

Thin Solid Films 638 (2017) 73–80

Contents lists available at ScienceDirect

Thin Solid Films

journal homepage: www.elsevier.com/locate/tsf

Analysis of polydihydrosilane crystallization by excimer laser annealing

Miki Trifunovic [a,*], Paolo Maria Sberna [a], Tatsuya Shimoda [b], Ryoichi Ishihara [a]

[a] Department of Electronic Components, Technology and Materials, Delft University of Technology, Feldmannweg 17, 2628CT Delft, The Netherlands
[b] School of Materials Science, Japan Advanced Institute of Science and Technology, 1-1 Asahidai, Nomi, Ishikawa 923-1292, Japan

ARTICLE INFO

Article history:
Received 23 May 2017
Received in revised form 7 July 2017
Accepted 14 July 2017
Available online 15 July 2017

Keywords:
Polydihydrosilane
Excimer laser crystallization
Solution-process
Ultraviolet curing
Finite-element analysis

ABSTRACT

Printing of electronics has been gaining a lot of attention over the past decade as a low cost alternative to conventional electronic fabrication methods. A significant development in this area was the possibility to print a silicon precursor, polydihydrosilane, which can directly be transformed into polycrystalline silicon by an excimer laser treatment. Due to the limited laser heat diffusion, low-cost flexible substrates such as plastics and even paper could be used that typically have low thermal budgets. Since the silicon precursor is sensitive to ultraviolet light and may transform in a photochemical reaction, the question arises whether the excimer laser crystallization is predominantly photochemical or rather a thermal reaction. In this work, a model is developed and reflected to experimental data, to understand the physics behind the process. Through finite-element analysis and experimental characterizations it was observed that the physics behind the process was predominantly thermal, and that instead of an intermediate transition to a-Si, a direct transformation to poly-Si exists. By understanding this process, the treatment can be optimized or more efficient tools can be used that would enable a low cost production of high performing silicon devices.

© 2017 Elsevier B.V. All rights reserved.

1. Introduction

While silicon is the dominant material in today's micro-and nanoelectronics industry, as a result of the vast advantages of printable electronics, research has placed a predominant focus on alternatives to silicon that can easily be converted to inks. In particular, organic and metal-oxide semiconductors are vastly being researched in this field [1–3]. As semiconductors however, these materials lack in electronic device performance compared to polycrystalline silicon (poly-Si). They typically have lower field-effect mobilities (typically ~1 cm^2/Vs for organic, 10 cm^2/Vs for metal-oxides, and 100 cm^2/Vs for poly-Si), lower material stability, and lack a good balance between electron and hole mobilities, which obstructs their usage in energy efficient complementary metal-oxide semiconductor (CMOS) circuitry [4–6].

In 2006, a liquid precursor, cyclopentasilane (CPS), was reported [7] which can be converted to polycrystalline silicon after a UV curing, thermal annealing, and laser crystallization step. Although this allowed for the first time printing of silicon, the thermal annealing of at least 350 °C, formed a limiting factor in this process preventing the application of the material to low-cost flexible substrates that typically have a low thermal budget. In recent years however, it has been reported [8] that after curing the silicon precursor, the material can directly be crystallized by an excimer laser treatment, thereby avoiding the heating of the substrate. The excimer laser is a high intensity ultraviolet (UV) light source that is typically used in the semiconductor industry for the annealing of thin films without affecting the bulk material. This has led to application of the liquid silicon precursor on top of low-cost, flexible substrates such as polyethylene terephthalate (PET), polyethylene naphthalate (PEN) and even paper. Since the silicon ink reacts to UV light for curing, a question arises whether the excimer laser crystallization process of the silicon ink is predominantly thermal or photochemical. Therefore, in this work, crystallized samples are analyzed and compared to a simulation model.

2. Experimental details

2.1. UV photopolymerization of cyclopentasilane

The conversion from CPS, to poly-Si requires an intermediate polymerization step. CPS molecules undergo a ring-open polymerization into polydihydrosilane (polysilane), and in this process release hydrogen and low mass silane radicals [9]. The ring-opened molecules form chains and cross-links with their neighboring ring-opened molecules [10]. Depending on the intensity of the UV curing light source, hydrogen content and cross-linking density of the material can be controlled. A comparison between CPS films exposed to an intensity of 10 mW/cm^2 (similar to related works [8,11,12]) and 300 mW/cm^2 has been made by analyzing the Raman spectra and absorbance over time in open air. The results are presented in Fig. 1. At a UV intensity of 300 mW/cm^2, an increased stability toward oxygen, and a stronger amorphous silicon signal was observed. Additionally, a change in color from transparent to

* Corresponding author.
E-mail address: m.trifunovic@tudelft.nl (M. Trifunovic).

http://dx.doi.org/10.1016/j.tsf.2017.07.038
0040-6090/© 2017 Elsevier B.V. All rights reserved.

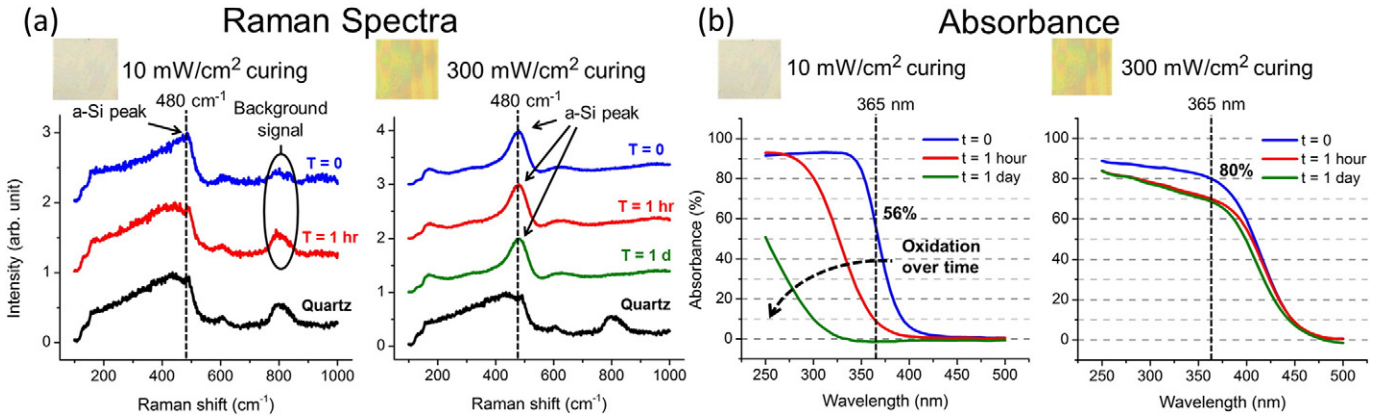

Fig. 1. A comparison in stability between two polysilane samples that have been cured with a different intensity for 30 min. A comparison in Raman spectra over time in (a), and a comparison in absorbance over time in (b).

yellow was evident, which is caused by the bandgap narrowing of the material [13]. Ablation of hydrogen and silane radicals as a result of subsequent laser crystallization is thereby significantly reduced. Therefore, in this work, CPS cured with a UV intensity of 300 mW/cm^2 is taken as the starting material for crystallization and has been further studied.

2.2. Modeling excimer laser crystallization of polysilane

In solid silicon, laser crystallization is a thermally dominated process. This is because the incident light generates electron-hole pairs which by their intra-band thermalization and non-radiative recombination create phonons. This is the case for laser energies exceeding the band gap energy, $h\nu > E_g$ (excimer laser > 3.4 eV, polysilane bandgap ≈ 2.5 eV). In addition, for nanosecond pulse durations, common in excimer laser systems, thermal models are most commonly used since photo-generated charges thermalize before far diffusion in the material, and therefore establish a local equilibrium within the lattice [14,15].

In this work, a KrF excimer laser (248 nm, 20 ns) has been used for the polysilane crystallization. A simulation model has been constructed which considers the temperature-space profile evolution within the irradiated film that has a continuous material structure. The model is restricted to the surface heating path of the film cross-section (1D), since the laser beam spot size (2×2 mm^2) is much larger than the thermal diffusion length (few hundred nanometers to micrometers) and the fluence within the spot is uniform. The model considers 200 nm of polysilane on top of a 5 μm SiO_2 substrate. Although the physical samples used for this work had a larger substrate thickness of several 100 μm, it was observed through simulations that the difference is significantly small to allow this simplification. The polysilane film is modeled with mesh elements of 0.1 nm in size, the substrate has a coarser mesh size of 1 nm since the absorption of the laser light occurs solely within the silicon ink film. Each mesh element is subject to classical thermal transport equations. Details on the use of equations are stated in Appendix A.

Details of parameter extraction from polysilane are presented in the Appendix B. Table 1 summarizes the value of the necessary simulation parameters of polysilane and molten silicon, and compares them to parameters used for the simulation of amorphous silicon performed in related works [16].

3. Results

Experimental results have indicated that the melting threshold of polysilane lies between 50 and 60 mJ/cm^2. Fluences around this threshold energy density have been simulated, that is: 50, 60, and 70 mJ/cm^2. The simulation results are compared to SEM images and Raman spectroscopy data of physical samples. Results of single pulse irradiation are presented in Fig. 2.

3.1. Single pulse laser treatment results

At a laser fluence of 50 mJ/cm^2, the melting temperature of 1440 K has almost been reached with a simulated maximum temperature of 1411.7 K. At this temperature, the material has softened. A small change in surface morphology is visible in the SEM image showing a wavy texture. The Raman spectrum shows an increase in the a-Si signal compared to a non-treated sample, but no crystalline signal is observed.

At a laser fluence of 60 mJ/cm^2, the melting temperature has been reached. A further significant increase in temperature is prevented since the film melting absorbs heat (latent heat of fusion) at a constant temperature of 1440 K. Surface morphology has significantly changed: bead shaped structures have formed from the agglomerating molten film as a result of surface free energy minimization of the liquid material. The Raman spectrum shows a visible crystalline silicon peak (crystalline fraction Xc = 39%), with an amorphous silicon shoulder, indicating the presence of both material types inside the film.

At a laser fluence of 70 mJ/cm^2, similar to the case of 60 mJ/cm^2, the temperature of the surface does not further increase significantly due to the phase change and surface morphology did not change. In this case, the Raman spectrum indicated a much stronger c-Si peak (crystalline fraction Xc = 90%) overwhelming the a-Si signal due to the doubling of the melt depth, as simulated. Although higher laser fluences in

Table 1
Parameters of polysilane, molten silicon and LPCVD a-Si, used for heat-transfer simulations at a laser wavelength of 248 nm.

Parameter	Polysilane	Molten silicon	a-Si:H
Melting point (K)	1440	–	1440
Density (g/cm^3)	2.1	2.52	2.26
Latent heat (J/g)	1320	–	1320
Absorption coefficient (cm^{-1})	$2.5 \cdot 10^{-5}$	$1.63 \cdot 10^{6}$	$1.75 \cdot 10^{6}$
Reflectivity	0.1	0.72	0.58
Heat capacity (J/kgK)	1600	860	952 + 0.0917 T
Thermal conductivity (W/mK)	0.7	50.2 + 0.0293(T-1687)	$1.3 \cdot 10^{-9}(T-900)^3 + 1.3 \cdot 10^{-7}(T-900)^2 + 1.0 \cdot 10^{-4}(T-900) + 1$

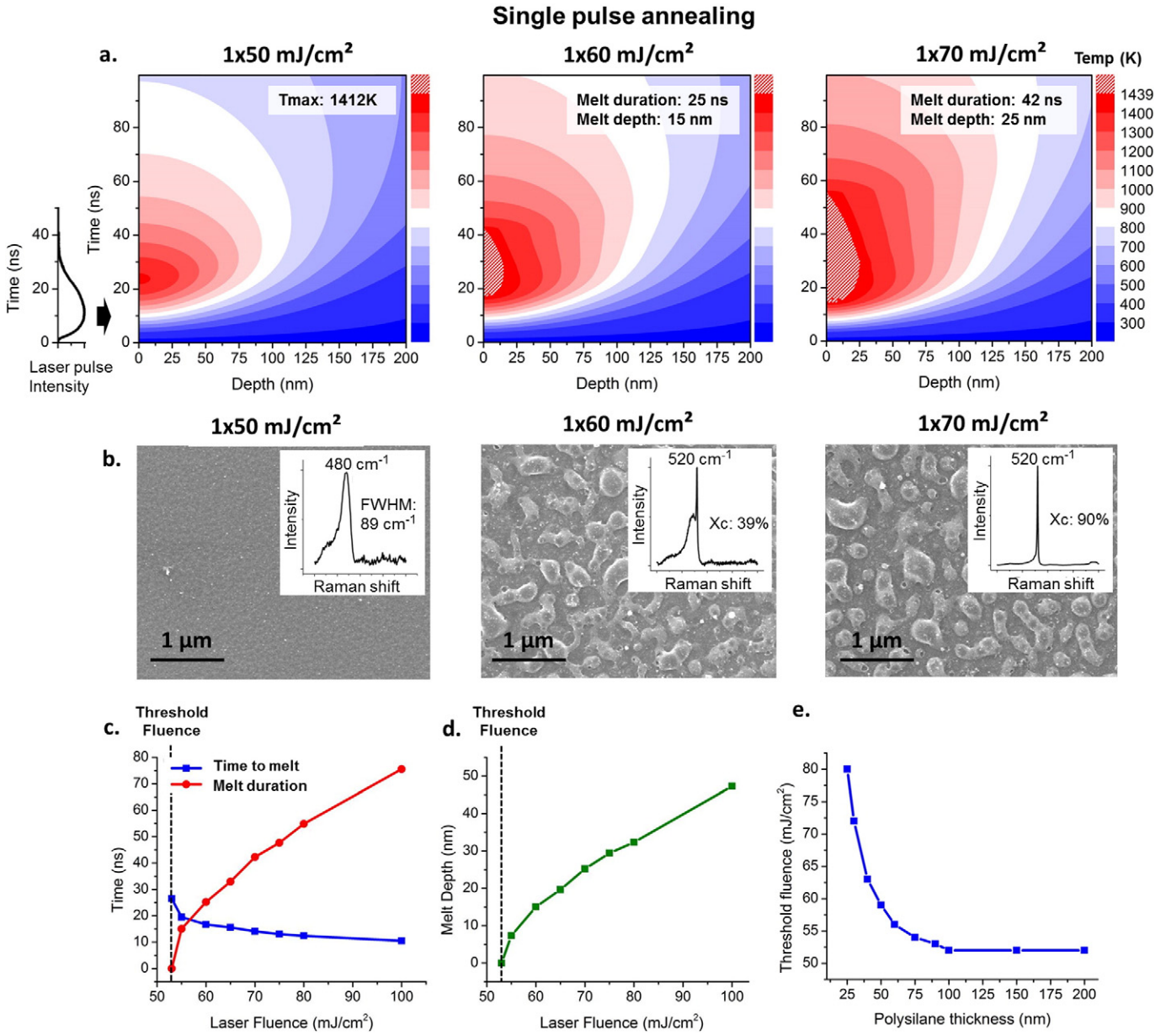

Fig. 2. Single pulse polysilane crystallization analysis. Finite element simulation results (a), SEM images of physical samples with their respective Raman spectra (b). Simulation results of time-to-melt and melt-duration (c), melt-depth (d), and thickness dependency on the threshold fluence (e).

general lead to bigger crystal grains, strong degassing and ablation effects are triggered, which adds to the increase in surface roughness and would hamper electronic device performance.

The time-to-melt decreases with increasing laser fluence, as shown in Fig. 2c. The curve decreases and saturates to 11.2 ns which is the time necessary for the laser pulse to reach its peak. For the melt duration, a proportional increase to the laser fluence is observed. Fig. 2d shows that the melt depth also increases proportionally to the laser fluences, although from a certain energy the effect of the SiO_2 interface will start to play a role and will decrease the speed of melt depth progression. Explosive crystallization in these simulations has not been taken into account, and these would increase the actual melt duration and depth.

When the thickness of the polysilane film reduces, the SiO_2 interface gets closer to the heated surface, allowing heat to transfer more easily to the substrate which cools the sample to a certain extent. There is a minimum polysilane thickness of approximately 100 nm, from which the threshold fluence does not change as a result of full energy absorbance. Effects other than the threshold fluence, for higher energy densities, may still change depending on the film thicknesses. The simulation results of the threshold fluence associated to various polysilane thicknesses are presented in Fig. 2e.

Compared to LPCVD a-Si simulations, the laser energy absorbed by the film is significantly higher as a result of the combination of optical and thermal properties of the polysilane film. Therefore, the melting temperature for polysilane was reached at much lower laser fluences. A threshold fluence of 52 mJ/cm^2 was found for polysilane (69 mJ/cm^2 for LPCVD a-Si). In addition, the melt depth is larger, resulting in a much larger crystalline fraction after the laser treatment. This indicates that an out-of-equilibrium transition from polysilane to polycrystalline silicon is in effect, and an intermediate transition to a-Si is unlikely to occur, since the properties of a-Si do not allow its crystallization at such low fluences.

3.2. Multiple pulse laser treatment results

For samples exposed to multiple laser pulses, a change in the starting material needs to be considered. For the case of high laser energy densities, where the starting material changes to poly-Si after the first pulse, the film will increase its crystallinity fraction as more pulses are irradiated. For laser fluences below but close to the threshold, while a single pulse does not reach the melting temperature, multiple pulses of the same fluence have revealed crystallization of the film. This was the case for a laser fluence of 50 mJ/cm^2, and is attributed to the outgassing of the a-Si film causing a decrease in material density. This allowed the melting temperature to be reached after exposure to subsequent laser pulses. A reduction in density from 2.1 g/cm^3 to 1.9 g/cm^3 is applied for these simulations, since the rise in temperature from the initial pulse leads to hydrogen and radical evaporation from the material. Melting temperature for this lower density film is now reached at the same 50 mJ/cm^2 fluence as shown in Fig. 3, in agreement with experimental data. Physically, this density change may not be sudden, and it may therefore take more than a second pulse to crystallize the film, depending also on the material conditions. For multiple pulses at even lower fluences, the polysilane is being annealed, and transforms into a-Si. As a result, the film does not reach the melting temperature, due to increases in density, decrease in heat capacity, and increase in thermal conductivity. This is further explained in the Appendix C. Although the change in density was used as a first approximation, other parameters will change as well. When density is decreased, it is likely to assume that the material also reduces its thermal conductivity, which would increase the film heating. At the same time, absorption and heat capacity will decrease, and lead to an overall decrease in film temperature. As a first approach, a decrease in density suffices, but a well-balanced combination should reach the melting point at 50 mJ/cm^2 which would reflect on the experimental results.

4. Discussion

Variations on laser type, starting material, and crystallization environment all have an impact on the crystallization result. A variation in wavelength and pulse duration changes the absorption of the light and duration of treatment and therefore changes the threshold fluence. The starting material may be manipulated by the curing process, which would effectively lead to a variance in material parameters. The simulations have accounted for a nitrogen environment. When the sample is treated in vacuum however, temperatures would significantly increase due to the absence of convective cooling.

This model can approximate the behavior of polysilane in the laser crystallization process but has a number of limitations that require attention. The simulation accuracy is largely dependent on the material parameters which are not easily extracted due to the strong sensitivity of the material to the open air. Approximations had to be made in some cases by using materials with similar properties such as polysilane annealed at 300 °C and polyethylene. Some physical features are left out in the simulation such as hydrogen outgassing and material evaporation which play strong roles in the polysilane crystallization process. This outgassing is accounted for by the decrease in density in the multiple pulse section, however, the model does not include the dynamic loss in energy due to this outgassing. Additionally, since the simulations in this work describe the evolution of the system up to the melting point, the crystallization process during the cooling down is not described, since the employed equations only describe the cooling down without nucleation and crystal growth dynamics. Therefore crystallization phenomena such as explosive crystallization, where the molten film surface propagates deeper inside the film as a result of latent heat production and propagation, has not been modeled, and an actual melt depth and duration may therefore be higher than the simulated results suggest. Finally, the model only focuses on thermal effects from the UV laser light and has shown a good agreement to the experimental results, indicating the dominance of this physical effect on the laser crystallization process of polysilane. Photochemical effects by the irradiated UV light however will also have a minor role in the material transformation process, and this has not been added to the model. Despite these limitations, this model gives a good indication on the physics behind the excimer laser crystallization of polysilane.

5. Conclusion

In summary, we have analyzed the excimer laser crystallization of polysilane through finite-element analysis and experimental characterizations. Although polysilane transforms into an a-Si 3D network photochemically due to UV light, the thermally induced transformation from the excimer laser is overwhelming. The melting temperature is reached at relatively low fluences. Fluences of 50, 60 and 70 mJ/cm^2 were analyzed, and compared to experimental data. The melting temperature is reached for fluences higher than 52 mJ/cm^2, and this was similar to the experimental data findings. Compared to LPCVD a-Si that has a melting threshold of approximately 69 mJ/cm^2, a much lower threshold was found, therefore it is

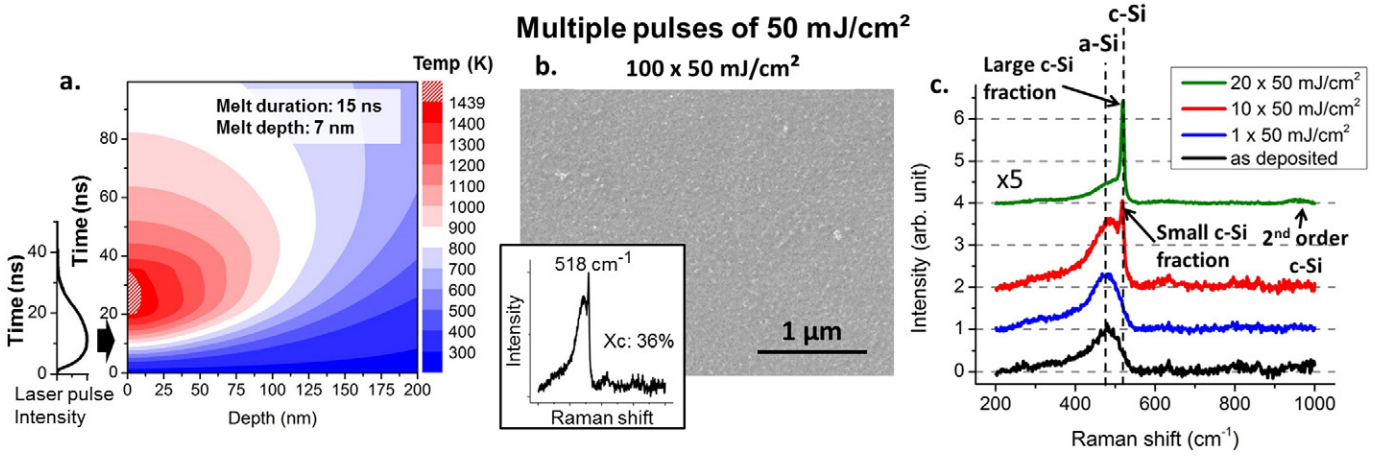

Fig. 3. Simulation and measurement results of the polysilane crystallization through multiple excimer laser pulses. Finite-element-simulation results (a), SEM image with respective Raman spectrum (b), different Raman spectra of various excimer laser pulse treatments (c).

unlikely that the polysilane material transforms into a-Si in an intermediate step.

The film may crystallize after irradiating multiple pulses at fluences slightly below the threshold. Simulations were conducted by increasing the porosity of the starting material as a result of the initial laser pulse and confirmed this crystallization.

Limitations in this model consist of the accuracy in the parameters used for the polysilane, the omission of physical phenomena such as energy loss during outgassing of the material, explosive crystallization, and the photochemical effect.

The model used in this work is based on a thermal model. Despite the omission of photochemical effects, the model shows a good agreement to experimental data, indicating the overwhelmingly dominating role of thermal over photochemical effects in this process.

Acknowledgements

We thank the technical staff of Else Kooi Laboratory for discussions and technical support. We would also like to thank Prof. Stephen Picken and Ben Norder from the Advanced Soft Matter department that have helped with the DSC measurements and discussion. This research did not receive any specific grant from funding agencies in the public, commercial, or not-for-profit sectors.

Appendix A. Heat transport equations

Heat absorption and transport induced by laser absorption is described by the one dimensional Stefan equation [14–16]:

$$\frac{\partial T}{\partial t} = \frac{\alpha}{\rho \cdot C_p} I(x,t) + \frac{1}{\rho \cdot C_p} \frac{\partial}{\partial x}\left(\kappa \frac{\partial T}{\partial x}\right) \tag{A1}$$

where, $\frac{\partial T}{\partial t}$ is the transient term, and accounts for the non-stationary behavior of temperature, and $I(x,t)$ is the absorbed power density of the laser pulse at depth x and time t. Properties of the treated material are reflected in the equation as: α the absorption coefficient, ρ the density, C_p the specific heat, κ the thermal conductivity, and $\frac{\partial T}{\partial x}$ accounts for the heat conduction in the solid.

Since it is assumed that the material is uniformly absorbing, the power density can be described by the Beer-Lambert law:

$$I(x,t) = I_0(t)(1-R)e^{-\alpha \cdot x} \tag{A2}$$

where I_0 is the output power density of the laser and R is the reflectivity of the material. This equation does not take into account the temperature dependence of the refraction index and the extinction coefficient that play a role in the reflectivity and absorption coefficient of the material.

The boundary condition at the bottom of the system is a fixed temperature of 293.15 K (Dirichlet condition), since the sample is always placed on a metallic chuck during laser annealing. The boundary condition at the top of the system is described by:

$$\vec{n}\left(\kappa \frac{\partial T}{\partial t}\right) = h(T_{ext} - T) \tag{A3}$$

where n is the unit vector, normal to the surface, h the convective heat transfer coefficient, and T_{ext} the constant ambient temperature of 293.15 K. For h, a value between 1 and 100 W/m^2 K is common for open air. In this work, a value of 1 W/m^2 has been used since the treatment is conducted within a confined ambient, although variations of this value has a negligible effect on the final simulation result.

In order to account for a smooth phase transition from polysilane to molten Si, a Heaviside step-function is triggered when the sample temperature increases above the melting point. Additionally, latent heat is implemented for the phase change from solid a-Si to molten silicon. A Gaussian curve is used with a standard deviation of 0.5 K, which allows a smooth transition of the latent heat around the melting temperature. The laser pulse time profile used in this simulation is based on an extraction from a physical excimer laser source. The solver time-step of the simulation is 0.1 ns.

This model assumes that melting and solidification occur at equilibrium phase-change temperature and that the introduction of interfacial kinetics into the modeling is not necessary.

Appendix B. Polysilane parameter extraction

Polysilane used for crystallization analysis in this work is prepared first by curing pure CPS for 30 min under a UV light with intensity of 10 mW/cm^2, followed by a UV curing of 300 mW/cm^2 for 30 min at 80 °C. Since a self-capping effect is present when curing with higher intensities, a weakly cured bulk is still present deeper inside the film. The capping layer is approximately 70 nm (penetration depth at 365 nm wavelength). The bulk of the excimer laser energy will be absorbed by this part (penetration depth of 40 nm at 248 nm wavelength) which makes the extracted parameters still relevant as simulation data although the model takes into account structurally uniform geometries. Values used in the simulation model are either extracted from measurement data or approximated by using values for comparable materials. These values are used as a first approximation and are subject to adjustments when reflected on experimental data of the crystallized samples.

B.1. Absorption coefficient and reflection

Transmission, reflection and absorbance of polysilane have been measured using the Lambda 950 (PerkinElmer) spectrophotometer equipped with a total integrating sphere (TIS). The sample was prepared on a quartz substrate. The absorption coefficient for polysilane is $2.5 \cdot 10^5$ cm^{-1} for the KrF wavelength of 248 nm, and is calculated by:

$$\alpha = -\frac{1}{d}\ln\left(\frac{T}{1-R}\right) \tag{F4}$$

Reflectance at this wavelength was found to be 10%. The absorption spectrum and reflectance are shown in Fig. B1.

B.2. Density

For the density of polysilane cured with 300 mW/cm^2 a value of 2.1 g/cm^3 is chosen. This is due to the strong similarity in both Raman as well as absorption spectra between this sample and the sample created by Masuda et al. which was annealed at 300 °C [13]. The density for this sample was found to be approximately 2.0 to 2.1 g/cm^3.

B.3. Heat capacity

Heat capacity has been measured using differential scanning calorimetry (PerkinElmer DSC7), where a heated sample is monitored while being compared to an equally heated reference. For these measurements 10 μL of CPS was poured into a small aluminum container and was cured for 30 min under 10 mW/cm^2 UV light. Subsequently the sample was cured with the stronger 300 mW/cm^2 UV light for 30 min at 80 °C. The container was air-tight sealed and brought outside of the glovebox for measurements. Fig. B2 shows the results of the DSC measurements. The initialization of the experiment caused the first heat capacity jump from 0 to approximately 1.6 J/gK close to room temperature. A thermal dependence was found when the temperature is further increased. This thermal dependence of heat capacitance is much stronger for the polymer (≫1.11 J/kgK) than for a-Si(0.0917 J/kgK) [16]. The measurement range however, was limited up to 150 °C since the material would slowly transform into amorphous silicon for increasing

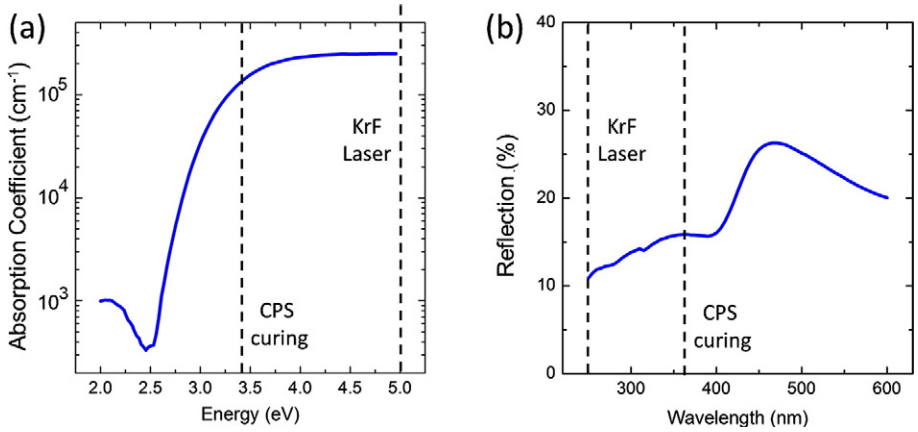

Fig. B1. Absorption spectrum (a), and the reflectance (b) of 200 nm thick polysilane cured with an intensity of 300 mW/cm^2.

temperatures as a result of cross-linking. Due to the slow temperature increment of the measurement setup of 10 °C per minute, the gradual increase of the specific heat is likely a result of the change of material properties. The polysilane exposed to the laser light however, would rapidly heat up to over a 1000 K in a few nanoseconds, thus it will not have time to undergo the transition into a-Si, and a strong thermal dependence such as the one observed is unlikely to occur.

Polyethylene is similar to polysilane with the same monomer structure, but instead of silicon atoms as the molecular backbone, carbon atoms are present. Because it has a similar structure to polysilane, it will form a good reference for parameter comparison. The heat capacity of polyethylene is 1900–2300 J/kgK (high density-low density). The measured heat capacity of 1600 J/kgK is similar but lower due to two important reasons: First, the polysilane found in the bulk of the measured content, is branched. It is more branched than the low density polyethylene (1–3% of carbon atoms [17], as opposed to approximately 20% for polysilane [10]), which as a result would decrease the heat capacity of a polymer. The second reason is that a high intensity curing treatment is employed to more strongly cross-link the top fraction of the measured polysilane. If this value is close to the one of a-Si (»980 J/kgK) the total value should be somewhat lower. A fixed heat capacity of 1600 J/kgK as observed from the DSC measurement results.

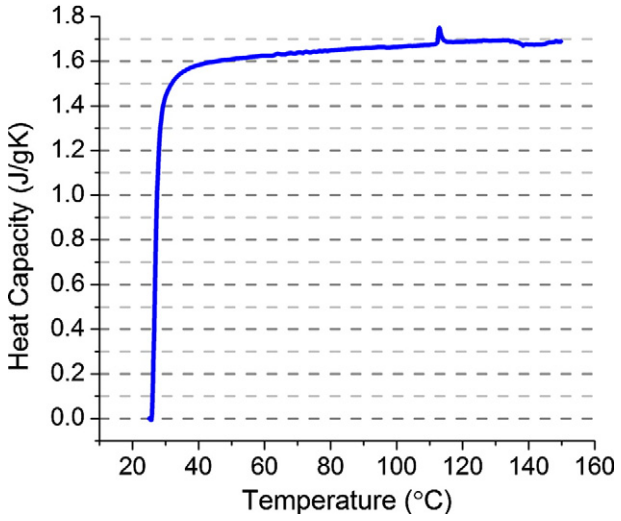

Fig. B2. Differential scanning calorimetry measurements of polysilane.

B.4. Melting temperature and latent heat

In general the melting point of a material is strongly depending on its molecular structure. The molecular weight, spatial arrangement (packing density) and intermolecular interactions are key parameters in the melting point [18,19]. Polysilane chain sizes vary from approximately 10^2 to 10^6 g/mol [10], and a precise melting temperature is therefore difficult to define a-priori. Cross-linking also plays a strong role and the higher degree of cross-linking between the polysilane chains, the more it would behave as a-Si. Considering the heavily cured polysilane for these simulations, it has been concluded that the a-Si melting point of 1440 K is a reasonable starting assumption for the polysilane used in this work.

Latent heat of fusion is related to the phase change of the material. As a result, it is dependent on the melting point of the film. As a first approximation, the latent heat for hydrogenated amorphous silicon (1320 J/g) has therefore been chosen.

B.5. Thermal conductivity

For the thermal conductivity of the material, it was difficult to make accurate measurements since the measurement setup requires a large amount of material which would make the curing treatment not feasible. Thermal conductivity is dependent on the type of bonds in the material, since heat is transferred through lattice vibrations and free electrons. The carbon counterpart of polysilane, polyethylene, has a thermal conductivity that varies between 0.4 and 0.5 W/(m·K), depending on its density. Polysilane used in this work is more branched and cross-linked compared to polyethylene which would increase the thermal conductivity since it approaches the 3D connectivity of a-Si, which has a conductivity of 1 W/(m·K). A thermal conductivity of 0.7 W/(m·K) has therefore been chosen.

Appendix C. Excimer laser pre-annealing

Excimer laser crystallization allows the treatment of thin layers of silicon without the thermal damage of the substrate or underlying layers. This is due to the short pulse duration (few tens of ns), and the high absorption coefficient of silicon (10^{5-6} cm^{-1}). The crystallization is the result of the absorption of the laser light translated to a sharp temperature increase of the material. As a result, the melting point of amorphous silicon (1200 °C) is reached.

Silicon intended to be crystallized, generally has a high hydrogen content. This is due to its synthesis which is meant for low-

temperature processes. A PECVD Si deposition process commonly results in a hydrogen content of the a-Si film of approximately 10%.

When the excimer laser fluence is high enough (reaching the Si melting temperature), during the sharp temperature increase, the hydrogen explodes out of the film, known as ablation. This process leaves a very rough and damaged silicon film, which is detrimental to the performance of the final TFT devices.

Reducing the hydrogen content can reduce ablation. It would also allow even higher laser fluences to be irradiated on the film which would result in bigger crystal grains. This can be done by thermally annealing the hydrogenated silicon in a furnace above 400 °C for a few hours [20–22]. This, however, takes away the purpose of using an excimer laser crystallization method on top of low-thermal budget substrates.

An alternative for reducing the hydrogen content is to use the excimer laser itself at low laser fluences, which would avoid damage to the underlying temperature sensitive layers. Hydrogen ablation is only initiated from certain laser energy densities, generally reaching the film melting temperature. Exposing the film to fluences below this energy, does not melt the film, but removes the hydrogen content, especially at the film surface. The laser fluence can then be slowly increased to remove more hydrogen until the crystallization fluence is reached without significant damage from ablation. This has been shown by numerous other groups in the case of PECVD a-Si:H [23–25]. The hydrogen issue exists also in the case of liquid silicon, annealed at 350 °C. Zhang et al. therefore, used a thermal treatment of 650 °C to two orders of magnitude worth of hydrogen from the film (from 1021 to 1019 [H] cm^{-3}) [20]. This allowed higher laser fluences to be irradiated on the sample without ablation. Later, Zhang et al., replaced the thermal dehydrogenation treatment with a laser induced pre-annealing [12]. In this work, experiments have been conducted regarding the laser induced pre-annealing process, since polysilane has much more hydrogen than thermally annealed amorphous silicon, and high temperatures cannot be used.

SEM images have been analyzed from a film that has been pre-annealed with 100 pulses of 20 mJ/cm^2, followed by 100 pulses of 40 mJ/cm^2. After the pre-annealing treatment, the film morphology has not changed at an optically observable level. When exposing the pre-annealed film to a single pulse of 70 mJ/cm^2, the film gets a wavy texture, similar to when the untreated film is exposed to a single pulse of 50 mJ/cm^2. This proves that higher energy density pulses could be irradiated, without damage, on films that have had a laser pre-annealing treatment. For this particular pre-annealing treatment the film still agglomerates at higher energy densities of 100 mJ/cm^2. The SEM images of the pre-annealed samples are presented in Fig. C1.

When looking at Raman spectra, that for which a single pulse would have resulted in poly-Si now becomes a-Si. Although higher fluences can be irradiated after a pre-annealing laser treatment, even higher laser fluences are necessary in order to crystallize the film. This is due to the structural change that the material inhibits: The film first turns into a densified a-Si [26]. After this, the crystallization process requires higher fluences, while in the reactive polysilane case the fluence necessary for crystallization is relatively low. A trade-off has to be made between keeping polysilane as a highly reactive material, and preventing ablation.

In the manuscript, single pulse laser annealing treatments have been simulated and matched to the experimental results. In addition, the scenario for multiple pulses was discussed. It was concluded that multiple pulses would lead to a porous silicon material due to the release of silicon hydride radicals and hydrogen. Other effects may have also played a role at the same time, although the dominating effect would be the structural change in material density for a specific, threshold level laser fluence (50 mJ/cm^2).

When the polysilane is treated however at lower laser fluences, although dehydrogenation and material outgassing occurs, since the temperature for crystallization is not reached, material densification occurs. This is also found for processes where the a-Si is dehydrogenated in a furnace [20]. A transition toward strongly cross-linked a-Si is present at these lower fluences. Consequently an a-Si structure requires higher laser energy fluences in order to be rearranged into a crystalline silicon structure. Transient heat simulations confirm this increase in threshold fluence.

For the crystallization of polysilane, ablation plays a large role due to the high hydrogen concentration inside polysilane films (~67%). Exposing the film to laser energy densities below crystallization levels helps remove the hydrogen and silicon hydride radicals. As a result, higher laser fluences can be irradiated on the film without ablation. Simulation results matching with experimental data, suggest that the material transforms into a-Si rather than becoming porous. This is in contrast to multiple pulse exposures close to the threshold fluence at 50 mJ/cm^2. The pre-annealing fluence is low enough to increase the cross-linking of the film. Therefore, the threshold fluence is increased. Optimization of the excimer laser pre-annealing process is required to obtain a good balance between the removal of hydrogen, while maintaining the high reactivity of polysilane.

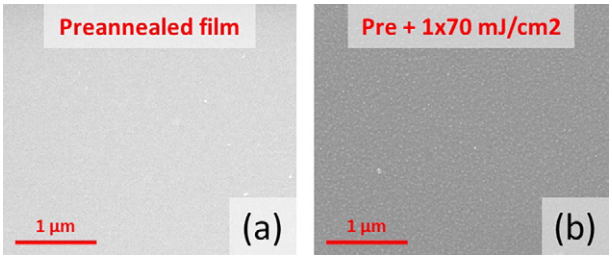

Fig. C1. SEM images of an excimer laser pre-annealed film (a), and a pre-annealed film with a subsequent exposure to 1 pulse of 70 mJ/cm^2 (b).

References

[1] W. Clemens, W. Fix, J. Ficker, A. Knobloch, A. Ullmann, From polymer transistors toward printed electronics, J. Mater. Res. 19 (7) (1963) 2004.
[2] J. Perelaer, P.J. Smith, D. Mager, D. Soltman, S.K. Volkman, V. Subramanian, J.G. Korvink, U.S. Schubert, Printed electronics: the challenges involved in printing devices, interconnects, and contacts based on inorganic materials, J. Mater. Chem. 20 (8446) (2010).
[3] S. Khan, S. Tinku, L. Lorenzelli, R.S. Dahiya, Flexible tactile sensors using screen-printed P(VDF-TrFE) and MWCNT/PDMS composites, IEEE Sensors J. 15 (6) (2015) 3146.
[4] J. Chang, T. Ge, E. Sanchez-Sinencio, Challenges of printed electronics on flexible substrates, IEEE 55th International Midwest Symposium on Circuits and Systems, IEEE 2012, pp. 582–585.
[5] E. Cantatore, Applications of Organic and Printed Electronics, Springer, New York, 2013.
[6] J.K. Jeong, The status and perspecties of metal oxide thin-film transistors for active matrix flexible displays, Semicond. Sci. Technol. 26 (2011), 034008. .
[7] T. Shimoda, Y. Matsuki, M. Furusawa, T. Aoki, I. Yudasaka, H. Tanaka, H. Iwasawa, D. Wang, M. Miyasaka, Y. Takeuchi, Solution-processed silicon films and transistors, Nature 440 (2006) 783.
[8] M. Trifunovic, T. Shimoda, R. Ishihara, Solution-processed polycrystalline silicon on paper, Appl. Phys. Lett. 106 (2015) 163502.
[9] A. Sugiyama, T. Shimoda, D.H. Chi, Ab initio study of the polymerization of cyclopentasilane, Mol. Phys. 108 (2010) 1649.
[10] T. Masuda, Y. Matsuki, T. Shimoda, Characterization of polydihydrosilane by SEC-MALLS and viscometry, Polymer 53 (2012) 3833.
[11] T. Masuda, N. Sotani, H. Hamada, Y. Matsuki, T. Shimoda, Fabrication of solution-processed hydrogenated amorphous silicon single-junction solar cells, Appl. Phys. Lett. 100 (2012) 253908.
[12] J. Zhang, M. Trifunovic, M. van der Zwan, H. Takagishi, R. Kawajiri, T. Shimoda, C.I.M. Beenakker, R. Ishihara, Single-grain Si thin-film transistors on flexible polyimide substrate fabricated from doctor-blade coated liquid-Si, Appl. Phys. Lett. 102 (2013) 243502.
[13] T. Masuda, Y. Matsuki, T. Shimoda, Pyrolytic transformation from polydihydrosilane to hydrogenated amorphous silicon film, Thin Solid Films 520 (2012) 6603.
[14] R.F. Wood, G.E. Giles, Macroscopic theory of pulsed-laser annealing. I. Thermal transport and melting, Phys. Rev. B 23 (2923) (1981).
[15] R. Černý, P. Přikryl, Modeling laser-induced phase-change processes: theory and computation, in: N.H. Nickel (Ed.), Laser Crystallization of Silicon – Fundamentals to Devices, vol. 75, Elsevier 2003, pp. 43–78.

[16] J. Förster, H. Vogt, Excimer laser-annealing of amorphous silicon layers, Proceedings of the 2011 COMSOL Conference, 2011 Stuttgart, Germany.
[17] X.M. Zhang, S. Elkoun, A. Ajji, M.A. Huneault, Oriented structure and anisotropy properties of polymer blown films: HDPE, LLDPE and LDPE, Polymer 45 (2004) 217–229.
[18] A.R. Katritzky, R. Jain, A. Lomaka, R. Petrukhin, U. Maran, M. Karelson, Perspective on the relationship between melting points and chemical structure, Cryst. Growth Des. 1 (2001) 261.
[19] M.R. Kamal, L. Feng, T. Huang, A generalized equation for the prediction of melting temperatures of homopolymers and copolymers, Can. J. Chem. Eng. 80 (2002) 432.
[20] J. Zhang, R. Ishihara, H. Takagishi, R. Kawajiri, T. Shimoda, C.I.M. Beenakker, Single-grain Si TFTs using spin-coated liquid-silicon, Tech. Dig. –Int. Electron Devices Meet, 2011 (14-51145-4).
[21] P. Boher, M. Stehle, B. Godard, J.L. Stehle, Single shot excimer laser annealing of amorphous silicon: Effect of hydrogen on the properties of the poly silicon, MRS Proc. 397 (1995) 417.
[22] K. Suzuki, M. Takahashi, M. Saitoh, Influences of hydrogen contents in precursor Si film to excimer laser crystallization, Appl. Phys. A Mater. Sci. Process. 69 (1999) S263.
[23] P. Mei, J. Boyce, M. Hack, R. Lujan, R. Johnson, G. Anderson, D. Fork, S. Ready, Laser dehydrogenation/crystallization of plasma-enhanced chemical vapor deposited amorphous silicon for hybrid thin film transistors, Appl. Phys. Lett. 64 (1994) 1132.
[24] D. Toet, P. Smith, T. Sigmon, T. Takehara, C. Tsai, W. Harshbarger, M. Thompson, Laser crystallization and structural characterization of hydrogenated amorphous silicon thin films, J. Appl. Phys. 85 (1999) 7914.
[25] V. Privitera, S. Scalese, A. La Magna, A. Pecora, M. Cuscunà, L. Maiolo, A. Minotti, D. Simeone, L. Mariucci, G. Fortunato, L. Caristia, F. Mangano, S. Di Marco, M. Camalleri, S. Ravesi, S. Coffa, M.G. Grimaldi, R. De Bastiani, P. Badalà, S. Bagiante, Low-temperature annealing combined with laser crystallization for polycrystalline silicon TFTs on polymeric substrate, J. Electrochem. Soc. 155 (2008) H764.
[26] P. Lengsfeld, N. Nickel, W. Fuhs, Step-by-step excimer laser induced crystallization of a-Si:H, Appl. Phys. Lett. 76 (2000) 1680.